Inorganic Chemistry
Cite This: Inorg. Chem. 2018, 57, 1846−1858
Article
pubs.acs.org/IC

Role of (1,3) {Cu-Cu} Interaction on the Magneto-Caloric Effect of Trinuclear {Cu^{II}-Gd^{III}-Cu^{II}} Complexes: Combined DFT and Experimental Studies

Mukesh Kumar Singh, Thayalan Rajeshkumar, Ravi Kumar, Saurabh Kumar Singh, and Gopalan Rajaraman*

Department of Chemistry, Indian Institute of Technology Bombay, Powai, Mumbai 400076, India

Supporting Information

ABSTRACT: Molecular refrigeration is found to be of great interest in the field of coordination chemistry, and Gd^{III} ion based complexes are particularly attractive, as they exhibit a large magneto-caloric effect (MCE). As the magnetic coupling in Gd^{III} clusters is difficult to control, other avenues to enhance the MCE values have been explored and incorporation of 3d metal ions in the cluster aggregation with Gd^{III} yielding {3d-Gd} clusters are targeted. Among the transition-metal ions, the Cu^{II} ion is particularly attractive, as it does not possess any anisotropy, and in this regard, several di- and polynuclear {Cu-Gd} clusters are reported to yield attractive MCE values. While the role of near-neighbor {Cu-Gd} interactions in the MCE has been explored in detail, how the next-nearest-neighbor interaction influences the MCE has not been explored. To explore the importance of next-nearest-neighbor (1,3) {Cu-Cu} interaction, we have undertaken detailed density functional studies on five trinuclear {Cu^{II}-Gd^{III}-Cu^{II}} complexes that are reported in the literature. In addition, we also report the synthesis and magnetic and EPR studies of a novel complex $[(CuSALen)_2Gd(NO_3)_3]$ (**6**; where SALen is *N*,*N*′-ethylenebis(salicylaldiminato)). Both magnetic and EPR studies reveal an $S = 9/2$ ground state for **6** with a very small zero-field splitting parameter (+0.01 cm^{-1}), which aid in the achievement of a large MCE value for this molecule. Magnetization data collected for **6** yield a magnetic entropy change ($-\Delta S_m$) of 17 J kg^{-1} K^{-1} at 3.5 K by employing a 7 T magnetic field. Our calculations on all six complexes reveal that {Cu-Gd} exchange is ferromagnetic in nature, while the next-nearest-neighbor {Cu-Cu} exchange is found to vary from a weak ferromagnetic to a moderate antiferromagnetic interaction. In all of the cases studied, simulated susceptibility data are in excellent agreement with the experimental data, offering confidence in the computed *J* values. In addition, we have developed a mechanism of magnetic coupling for {Cu^{II}-Gd^{III}-Cu^{II}} trinuclear complexes, where the role of formally empty 5d, 6s, and 6p orbitals of Gd^{III} ion is established. In particular, our studies reveal that the next-nearest-neighbor {Cu-Cu} interaction is strongly correlated to Cu−Gd−Cu angle, with both smaller and larger angles yielding stronger antiferromagnetic exchange. The antiferromagnetic {Cu-Cu} interaction diminishes the gap between the ground $S = 9/2$ state and first excited $S = 7/2$ state, leading to enhancement of MCE values. In contrast to the general belief that weak interactions are desired for large MCE, our study advocates targeting a stronger antiferromagnetic {Cu-Cu} interaction to obtain larger MCE values in this class of clusters.

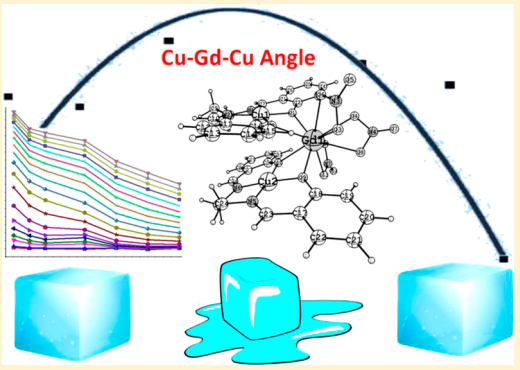

INTRODUCTION

Magnetic refrigeration, a potential application for low-temperature cooling, works on the principle of the magneto-caloric effect (MCE) via a magnetic cycle.[1] In this cycle, under adiabatic conditions, a change in the magnetic entropy denoted as $-\Delta S_m$ of the refrigerant upon removing the magnetic field is the key parameter that defines the performance.[2] Although the initial discovery of MCE has been on solid-state materials, there has been a recent surge of utilizing molecules for refrigeration purposes, as in many cases they are found to be superior to the alloys tested.[3] There are several prerequisites for achieving large $-\Delta S_m$ values for molecules, and these include (i) a large spin ground state, (ii) very small or no anisotropy, and (iii) large metal/ligand mass ratio, which maximizes the unpaired electron density. In addition to these factors, the nature of the magnetic coupling between the metal centers is also relevant, as ferromagnetic exchange between the metal centers leads to a high-spin ground state and a small exchange coupling constant ensures close-lying excited states, which helps to enhance the $-\Delta S_m$ values further. In particular, the gain in $-\Delta S_m$ values are significantly higher if the effective ground state of the molecule is degenerate in nature, as given by the equation $S_m = nR \ln(2S + 1)$ (where S_m = magnetic entropy, n = degeneracy, R = gas constant, and S = effective ground spin state).

Received: October 31, 2017
Published: February 1, 2018

DOI: 10.1021/acs.inorgchem.7b02775
Inorg. Chem. 2018, 57, 1846−1858

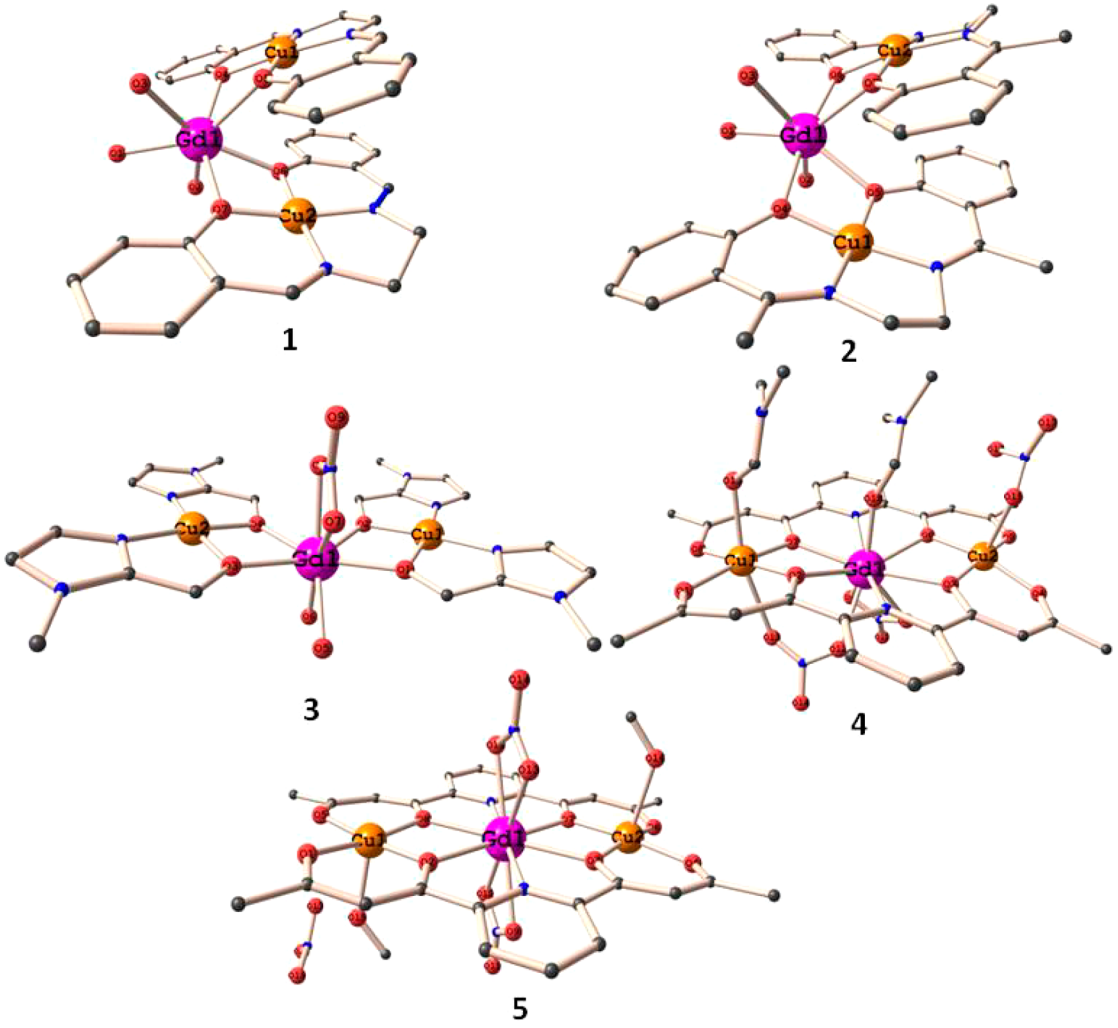

Figure 1. Molecular structures of complexes **1**−**5**. Color code: Gd, pink; Cu, golden yellow; O, brick red; N, blue; C, gray. H atoms are omitted for clarity.[12−15]

Among several metal ions, the Gd^{III} ion is particularly attractive, as it possesses seven unpaired electrons in the 4f orbitals and is isotropic in nature, satisfying the criteria for obtaining large MCE values.[4] For this reason, there are numerous examples reported with Gd^{III} ions possessing very large MCE values.[4,5] These examples include $\{Gd(HCOO)_3\}_n$, possessing a $-\Delta S_m$ value of 55.9 J kg^{-1} K^{-1} for an applied field change of ΔB = 7 T.[4b] Although the Gd^{III} ion possesses the maximum number of unpaired electrons, large clusters synthesized using Gd^{III} ions do not often result in large MCE values. This is essentially due to the fact that the magnetic coupling between two Gd^{III}-Gd^{III} ions is often very weak and can be either ferromagnetic or antiferromagnetic. If the exchange interaction between the Gd^{III}-Gd^{III} ions is antiferromagnetic in nature, this often leads to a diamagnetic ground state with no interesting MCE characteristics.[5c,6]

In search of rational improvement toward large MCE values, 3d metal ions have been incorporated into the cluster aggregation along with the isotropic Gd^{III} ion. This combination of {3d-Gd} cluster has several advantages: (i) the {3d-Gd} magnetic coupling is generally ferromagnetic in nature with a few exceptions[7] and (ii) several magneto-structural correlations are already available,[8] suggesting a possible way to fine-tune the J values in {3d-Gd} clusters. These key advantages have led to the birth of numerous {3d-Gd} clusters possessing attractive $-\Delta S_m$ values.[9] Among the 3d elements, the Cu^{II} ion is particularly attractive, as it is inherently isotropic with {Cu-Gd} magnetic exchange often found to be ferromagnetic in nature.[5f,9b,f,h,i,10]

Theoretical tools play a pivotal role in this area, particularly in computing the magnetic exchange constants and in understanding how they are correlated to the structural parameters.[8] This helps to find a way to fine-tune the J values and hence the $-\Delta S_m$ values. In addition, for polynuclear clusters possessing several exchange constants, it is impossible to extract the exchange coupling solely from the magnetic data and these are often estimated using computational tools.[6a,9a,10a,e,11] While building large {3d-Gd} clusters seems advantageous for attaining large MCE values, there are several issues still present, as the cluster topology cannot be controlled. For example, if there are {3d-3d} superexchange pathways in a cluster, they are often stronger, leading to a larger separation of spin levels and resulting in smaller MCE values.[10e] The presence of {Gd-Gd} exchange interactions which could be antiferromagnetic in nature also diminishes the overall MCE values. For these reasons, it is important to build a cluster assembly where {3d-Gd} interactions are maintained. There have been several such {3d-Gd}, {3d-Gd-3d}, and {3d-Gd-3d-

DOI: 10.1021/acs.inorgchem.7b02775
Inorg. Chem. 2018, 57, 1846−1858

Gd} clusters reported possessing attractive MCE values.[9,10] While this strategy seems attractive, there are apparent caveats: in {3d-Gd-3d} trinuclear clusters beyond the (1,2) {3d-Gd} interactions, there is also (1,3) {3d-3d} interaction present. This next-nearest-neighbor (1,3) interaction is often difficult to estimate from experiments and is frequently ignored in an attempt to fit the susceptibility data. When the {3d-Gd} interactions are very small, the (1,3) {3d-3d} interaction may play a prominent role in controlling the ground and the excited states. This issue has been largely unresolved in the literature.

To probe the correlation between the next-nearest-neighbor (1,3) {Cu-Cu} interaction with the structure and MCE properties, we have chosen five trinuclear {Cu^{II}-Gd^{III}-Cu^{II}} complexes from the literature. These are $[(CuSALen)_2Gd(H_2O)_3](ClO_4)_3\cdot 2CuSALen\cdot 0.5C_2H_5NO_2$, where Cu(SALen) is *N*,*N*′-ethylenebis(salicylaldiminato)copper(II) (**1**),[12] $[(CuHAPen)_2Gd(H_2O)_3](ClO_4)_3\cdot 2CuHAPen$, where Cu-HAPen is *N*,*N*′-ethylenebis(*o*-hydroxyacetophenoneiminato)-copper(II) (**2**),[12] $[Cu_2Gd(mmi)_4(NO_3)(H_2O)_2](ClO_4)(NO_3)\cdot 2H_2O$, where Hmmi is 2-hydroxymethyl-1-methylimidazole (**3**),[13] $[Cu_2Gd(L)_2(NO_3)_2(Me_2NCHO)_2]NO_3$, where H_2L is 2,6-bis(acetoacetyl)pyridine (**4**),[14] and $[Cu_2Gd(L)_2(MeOH)_2(NO_3)_3]$, where H_2L is 2,6-bis(acetoacetyl)-pyridine (**5**)[14,15] (see Figure 1 and Figure S1 in the Supporting Information). The synthesis, structure, and magnetic properties of these complexes have been reported earlier.[12−15] We are also additionally reporting here the novel complex $[(CuSALen)_2Gd(NO_3)_3]$ (**6**) (see Figure 2 and Figure S1 in the Supporting Information) and have characterized it using magnetic measurements and EPR spectroscopy. All six of these complexes have a {$Cu(OR)_2Gd(OR)_2Cu$} general structure motif, and therefore their magnetic and MCE characteristics can be compared. In particular, complexes **1**−**6** have been chosen in such a way that there is a large variation in the Cu−Gd−Cu angles (angles vary from 71.5 to 180.0°).

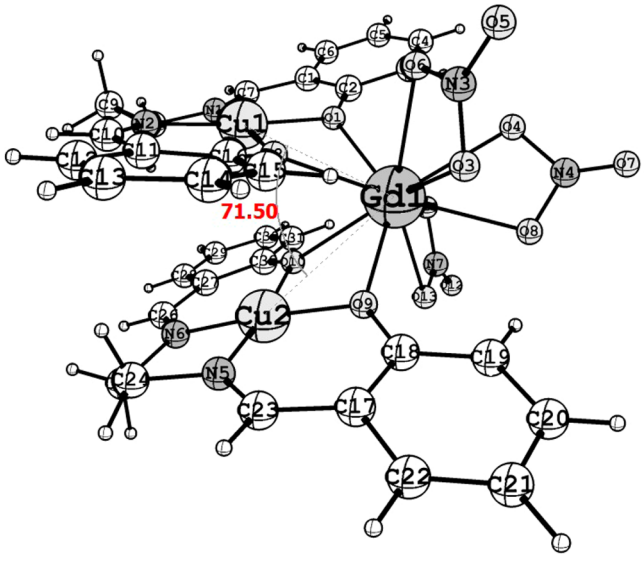

Figure 2. Crystal structure of complex **6**.

COMPUTATIONAL METHODOLOGY

Three different exchange pathways were modeled in complexes **1**−**6**. The exchange interactions between Cu^{II} and Gd^{III} ions are labeled as J_1 and J_2, whereas the next-nearest-neighbor interaction, between Cu^{II} ions, is labeled as J_3 (see Scheme 1). To evaluate the exchange interactions in **1**−**6**, the following exchange Hamiltonian has been employed:

$$\hat{H} = -[2J_1(S_{Gd}\cdot S_{Cu1}) + 2J_2(S_{Gd}\cdot S_{Cu2}) + 2J_3(S_{Cu1}\cdot S_{Cu2})]$$

Scheme 1. Schematic Representation of Exchange Pathways in Complexes 1−6

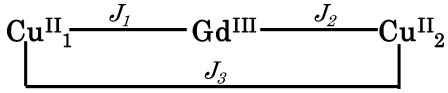

The energies of four spin configurations for **1**−**6** were computed to extract *J* values. From the energies of these spin configurations and expression of them through a pairwise interaction model, the exchange coupling constants have been estimated using the broken symmetry (BS) approach developed by Noodleman.[16] In accordance with our earlier method assessment for a {Cu-Gd} pair,[10e] we have employed the UB3LYP functional[17] in conjunction with a TZV basis set[18] for all atoms except for Gd, for which the relativistically corrected effective core potential (ECP) basis set of Cundari and Stevens (CSDZ)[19] was employed. All of the calculations were performed with the Gaussian 09 suite of programs.[20] To ascertain the error bar on the estimated *J* values, we have performed error analysis for selected complexes (**4**−**6** where $J_1 = J_2$). This yields very small errors of the order of 10^{-3} cm^{-1} on the estimated *J* values. The magnetic properties were simulated using the MAGPACK software,[21] and $-\Delta S_m$ calculations have been computed using PHI.[22]

EXPERIMENTAL STUDIES

In addition to the computational study, we have also synthesized a {Cu^{II}-Gd^{III}-Cu^{II}} cluster following the experimental procedure reported for the related structure.[12,23] All of the reactions were carried out under aerobic conditions with the analytical grade of solvents and reagents without further purification. A graphite monochromator (Mo Kα, λ = 0.71073 Å) was used in a Rigaku Saturn CCD diffractometer for single-crystal data collection. Selected crystals were mounted on the tip of a glass pin using mineral oil and placed in the cold flow produced with an Oxford Cryo-cooling device. Complete hemispheres of data were collected using ω and φ scans (0.3°, 16 s per frame). Integrated intensities were obtained with the Rigaku Crystal Clear-SM Expert 2.1 software, and they were corrected for absorption effects. Structure solution and refinement were performed with the SHELX package. The structures were solved by direct methods and completed by iterative cycles of ΔF syntheses and full-matrix least-squares refinement against F^2. See Table S1 in the Supporting Information for the crystallographic parameters of **6** (CCDC deposition number 1565951). The magnetic susceptibility measurements were obtained with the use of an MPMS SQUID magnetometer. The measurements were performed on polycrystalline samples, and the magnetic data were corrected for the sample holder and diamagnetic contribution. The magnetic data were fitted to complex **6** using the PHI software. Variable-temperature EPR spectra of compound **6** in frozen solution (toluene) were recorded using a Bruker spectrometer operating at X-band (9.5 GHz) frequency, and the EPR simulation was performed with Easyspin software (version 5.0.0).[24]

Synthetic Procedure. The copper Schiff base complex [*N*,*N*′-ethylenebis(salicylaldiminato)]copper(II) (CuSALen) was prepared as previously described.[25] A 2.0 mmol portion of gadolinium(III) nitrate was dissolved in ca. 20 mL of absolute hot ethanol. The copper complex (3.0 mmol) was dissolved in ca. 100 mL of hot chloroform. The two solutions were mixed. A light brick red precipitate was immediately formed, and the suspension was stirred at room temperature for 3−4 h. The precipitate was filtered, washed with chloroform−petroleum ether, and dried under vacuum. In an attempt to obtain crystals suitable for X-ray analysis, the compound was dissolved in hot nitrobenzene and the solutions were allowed to

DOI: 10.1021/acs.inorgchem.7b02775
Inorg. Chem. 2018, 57, 1846−1858

Scheme 2. Reaction Scheme Used for the Synthesis of Complex 6

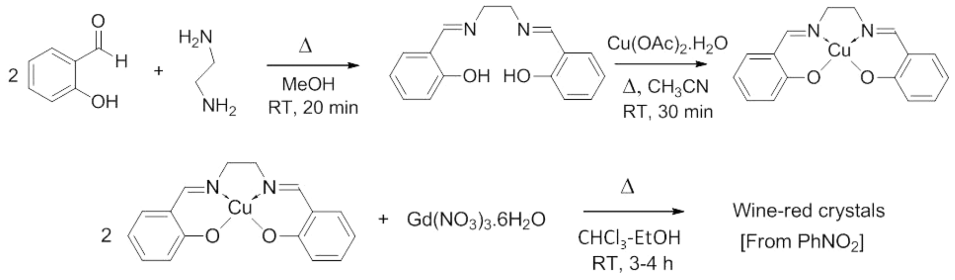

Table 1. Selected Structural Parameters in Relation to the J_1 and J_2 {Cu-Gd} Interaction of Complexes 1−6[12−15]

	av bond length (Å)		bond angle (deg)		dihedral angle (deg)	
complex						
1	Cu_1−μ-O	1.93	Cu_1−μ-O−Gd	101.0	Cu_1−μ-O−Gd−μ-O	12.9
				97.8	Cu_2−μ-O−Gd−μ-O	21.0
	Cu_2−μ-O	1.93	Cu_2−μ-O−Gd	102.4		
				97.8		
	Gd−μ-O	2.37	Cu_1−Gd−Cu_2	87.2		
2	Cu−μ-O	1.92	Cu_1−μ-O−Gd	102.8	Cu_1−μ-O−Gd−μ-O	12.4
				102.9	Cu_2−μ-O−Gd−μ-O	12.4
	Cu_2−μ-O	1.92	Cu_2−μ-O−Gd	102.8		
				102.9		
	Gd−μ-O	2.38	Cu_1−Gd−Cu_2	106.7		
3	Cu_1−μ-O	1.92	Cu_1−μ-O−Gd	105.7	Cu_1−μ-O−Gd−μ-O	1.9
				103.0	Cu_2−μ-O−Gd−μ-O	3.4
	Cu_2−μ-O	1.92	Cu_2−μ-O−Gd	105.5		
				102.7		
	Gd−μ-O	2.33	Cu_1−Gd−Cu_2	148.9		
4	Cu_1−μ-O	1.94	Cu_1−μ-O−Gd	106.8	Cu_1−μ-O−Gd−μ-O	11.3
	Cu_1−O(carboxylate)	2.68		108.3	Cu_2−μ-O−Gd−μ-O	5.7
	Cu_2−μ-O	1.93	Cu_2−μ-O−Gd	109.7		
	Gd−μ-O	2.54		108.2		
	Gd−O(carboxylate)	2.46	Cu_1−Gd−Cu_2	168.1		
5	Cu_1−μ-O	1.93	Cu−μ-O−Gd	110.0	Cu_1−μ-O−Gd−μ-O	0.7
				108.7	Cu_2−μ-O−Gd−μ-O	0.7
	Cu_2−μ-O	1.93	Cu_2−μ-O−Gd	108.7		
				110.0		
	Gd−μ-O	2.52	Cu_1−Gd−Cu_2	180.0		
6	Cu_1−μ-O	1.94	Cu_1−μ-O−Gd	101.1	Cu_1−μ-O−Gd−μ-O	19.4
				96.4	Cu_2−μ-O−Gd−μ-O	19.4
	Cu_2−μ-O	1.94	Cu_2−μ-O−Gd	101.1		
				96.4		
	Gd−μ-O	2.47	Cu_1−Gd−Cu_2	71.5		

evaporate at room temperature. Wine red crystals were formed in few days (see Scheme 2).

RESULTS AND DISCUSSION

Structural Description for Complexes 1−5. Detailed structural and magnetic characterizations of complexes **1−5** have already been reported.[12−15] In trinuclear {Cu^{II}-Gd^{III}-Cu^{II}} complexes, the gadolinium (Gd^{III}) ion lies between two copper (Cu^{II}) ions. The J_1 and J_2 interactions between Gd^{III} and Cu^{II} ions are mediating via two μ_2-oxo bridges, as shown in Figure 1. The coordination number around Cu^{II} ions is 4 (5-coordinated in the case of **5** and 5-/6-coordinated in the case of **4**), whereas the coordination number around the Gd^{III} ion varies from 7 to 10. The Cu−Gd−Cu angles are found to vary across complexes **1−6** as shown in Figure 1. The most important structural parameters that influence the {Cu-Gd} coupling are shown in Table 1. In particular, it has been shown earlier that the Cu−O−Gd angle and Cu−O−Gd−O dihedral angle are two prominent parameters that influence the exchange interactions in dinuclear complexes.[8a,10e] Here, the Cu−O−Gd angle is found to vary from 96.4 to 110.0° and the Cu−O−Gd−O dihedral angle is found to vary from 0.7 to 21.0° among the structures chosen.

Structural and Magnetic Characteristics of Complex 6. Complex **6** (see Figure 2) has a trimetallic Cu−Gd−Cu core which crystallized in a *Fdd*2/*P*1 space group. The gadolinium ion is 10-coordinate, with the geometry close to that of *sphenocorona J87*. The Cu^{II} ions possess a distorted-square-planar geometry (for a SHAPE analysis see Table S2 in the Supporting Information). To the best of our knowledge, the Cu−Gd−Cu angle of 71.5° in complex **6** is the smallest reported to date.

DOI: 10.1021/acs.inorgchem.7b02775
Inorg. Chem. 2018, 57, 1846−1858

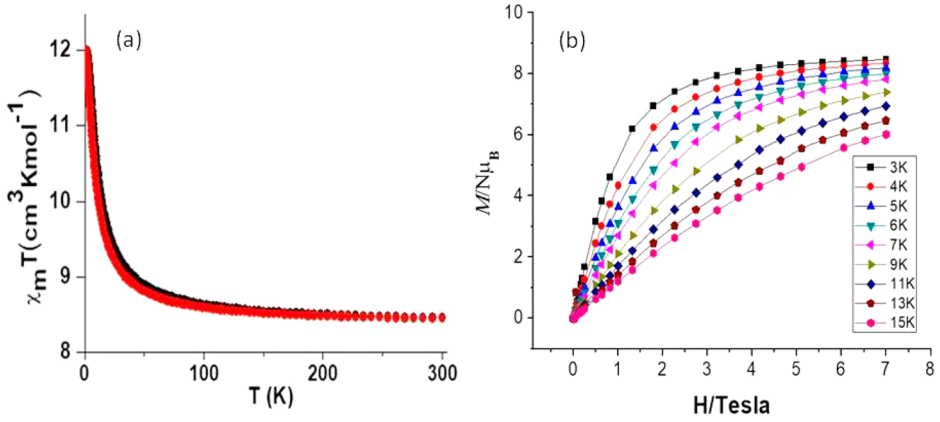

Figure 3. (a) Experimental (black squares) and simulated (red squares) magnetic susceptibility curves for complex **6**. (b) Field-dependent magnetization measurements performed on a polycrystalline sample of **6** at the indicated temperatures.

Table 2. Experimental and DFT Computed Exchange Coupling Constants (J_1–J_3) for Complexes 1–6, Along with the Cu–Gd–Cu Angle[12–15]

	J value (cm^{-1})								
	exptl			DFT calcd					
						J_3			
complex	J_1	J_2	J_3	J_1	J_2	Gd^{III}	La^{III}	La^{III} (54)	Cu–Gd–Cu (deg)
1	3.69	3.69	−6.12	3.22	2.01	−0.25	−1.05	−1.05	87.20
2	2.66	2.66	−2.10	3.40	3.19	0.14	0.47	0.32	106.69
3	2.88	2.88	1.99	3.86	3.78	0.01	1.26	1.71	148.89
4	1.40	1.40		0.88	0.95	−0.12	−0.67	−0.74	168.14
5	1.55	1.55		1.06	1.06	−1.15	−1.73	−2.20	180.00
6	1.46	1.46	−0.19	1.46	1.46	−0.19	−0.87	−0.86	71.50

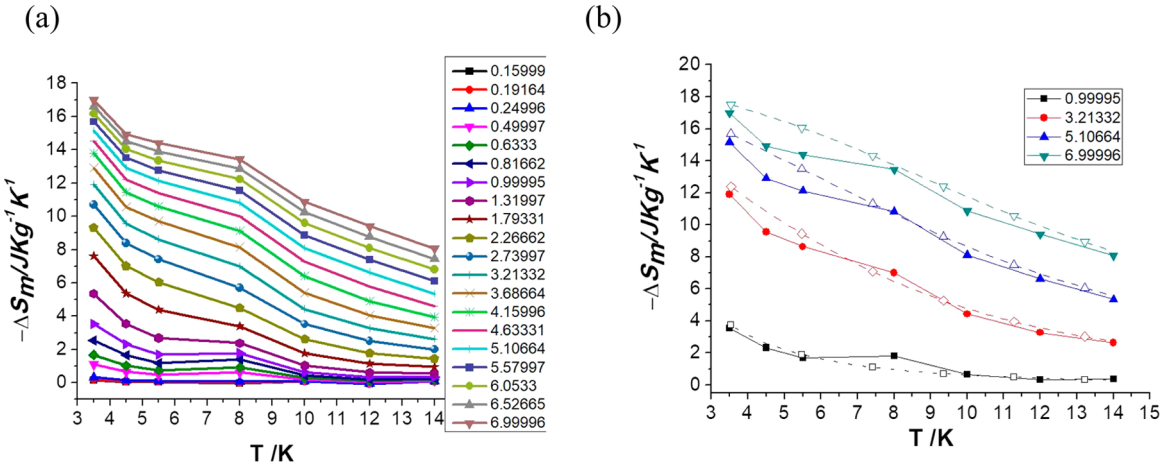

Figure 4. Change in magnetic entropy extracted from (a) the isothermal magnetization measurement and (b) the DFT simulated plot for complex **6**. In Figure 4b, solid lines represent experimental plots and dashed lines represent DFT simulated data.

Magnetic Measurements. Direct current (dc) magnetic susceptibility measurements have been performed on a polycrystalline sample of complex **6**, in a temperature range of 2–300 K (see Figure 3a). For complex **6**, the $\chi_M T$ value is found to be 8.51 cm^3 K mol^{-1} at 300 K, which is slightly lower than the expected value (8.63 cm^3 K mol^{-1}) for the three uncoupled metal ions (2 Cu^{II} and 1 Gd^{III}). At 9.2 K, the $\chi_M T$ value increases and reaches a maximum of 12.06 cm^3 K mol^{-1}, indicating a ferromagnetic interaction between Gd^{III}–Cu^{II} ions that results in S = 9/2 as the ground state for complex **6**. Isothermal field dependent magnetization measurements have been performed for complex **6** at different temperatures (3, 4, 5, 6, 7, 9, 11, 13, and 15 K, see Figure 3b). Complex **6** shows a sharp increase in magnetization value at low temperatures and low fields, suggesting a predominant population of the ground state.

At a high magnetic field, complex **6** saturates with a magnetization value of 8.5 Nμ_B. The observed saturation value of magnetization suggests an S = 9/2 ground state for complex **6**. The magnetic susceptibility data were simulated using DFT computed J_1–J_3 values, and this yielded an excellent match to the experimental data (see Figure 3 and Table 2). This suggests

DOI: 10.1021/acs.inorgchem.7b02775
Inorg. Chem. 2018, 57, 1846–1858

that the parameter-free fitting approach could be employed even for simpler clusters.

For complex **6**, we have performed detailed magnetization measurements from 3.5 to 14.0 K to estimate MCE values (see Figure 4). We have estimated the change in magnetic entropy ($-\Delta S_m$) using Maxwell's thermodynamic equation (eq 1):

$$\Delta S_m(T)_{\Delta B} = \int \left[\frac{\partial M(T, B)}{\partial T}\right]_B dB \quad (1)$$

As the magnetic field increases, the magnetic entropy increases and reaches a maximum value of 17.0 J kg^{-1} K^{-1} at 3.5 K (ΔB = 7 T).

Electron Paramagnetic Resonance Study for Complex 6. To ascertain the spin Hamiltonian parameters of the ground state, we have performed EPR measurements at X-band frequency. The frozen solution spectrum recorded at 5 K is shown in Figure 5 (for higher temperature spectra see Figure S2 in the Supporting Information). To estimate the spin Hamiltonian parameters, we have simulated the EPR spectra using the EasySpin suite[24] (version 5.0.0). In complex **6**, three spins S_{Gd} = 7/2 and S_{Cu1} = S_{Cu2} = 1/2 coupled to give rise the four total spin states S = 9/2, two S = 7/2, and one S = 5/2 according to the Kambe approach.[26] At higher temperatures, all of these states are expected to be populated and give a broad signal, as has been witnessed for **6**. At a temperature of 5 K, the spectrum resolves to exhibit several narrow lines centered around $g \approx 2.00$, suggesting a small zero-field splitting for the S = 9/2 ground state. We have attempted to simulate all the lines using S = 9/2 state; while all of the features are reproduced in our simulations, the signal observed at $g \approx 2.5$ is not reproduced. Temperature-dependent EPR studies reveal that this line loses intensity as the temperature decreases, suggesting that this is likely to arise from the excited state. The magnetic study reveals rather a weak coupling leading to the first excited S = 7/2 state at 9.8 cm^{-1} for this complex, and therefore we have additionally employed the S = 7/2 state to reproduce this feature. For the S = 9/2 state, simulation yields g = 1.99, D = 0.01 cm^{-1}, and E = 0.003 cm^{-1}, and for the S = 7/2 first excited state, g = 2.5, D = 0.18 cm^{-1}, and E = 0.022 cm^{-1} parameters are extracted (see the red and blue simulated graphs in Figure 5). Clearly, the EPR spectrum discloses that the ground state is S = 9/2, with the first excited state being S = 7/2. This suggests that the {Cu-Gd} coupling is ferromagnetic, as shown by the magnetic measurements. The estimated D value of the S = 9/2 state is rather small, and the rhombic anisotropy is negligible. This is rather expected, as the Gd^{III} ion is isotropic in nature with the Cu^{II} ion possessing no single-ion anisotropy. In addition, the **g** tensor is also isotropic in nature and all of these factors are favorable for the observation of large MCE values, as seen in the previous section. Interestingly, the zero-field splitting of the first excited state S = 7/2 is slightly large and this may be unfavorable for MCE values.

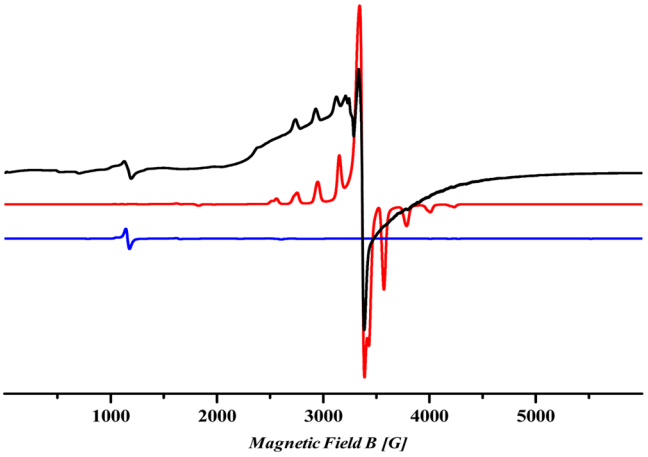

Figure 5. X-band EPR spectrum recorded on a polycrystalline sample of complex **6** at 5.0 K (black) and simulated spectra at S = 9/2 (for higher portion) (red) and simulated spectra at S = 7/2 (for lower portion) (blue). The parameters used for the simulation are g = 1.99, D = 0.01 cm^{-1}, and E/D = 0.30 for S = 9/2 and g = 2.5, D = 0.18 cm^{-1}, and E/D = 0.12 for S = 7/2.

Exchange Pathways. DFT computed exchange interactions for complexes **1**–**6** are shown in Table 2. The J_1 and J_2 interactions are found to be ferromagnetic in nature for all complexes. Magnitudes of the computed {Cu-Gd} interactions are in accord with expectation and earlier studies.[8a,10e] For complexes **4** and **5**, the next-nearest-neighbor {Cu-Cu} interaction has not been taken into account on fitting the magnetic data (see Table 2). To see how the DFT computed J values reproduce the experimental data reported earlier,[12−15] we have simulated the χT versus T data using DFT J values and this is found to excellently match with experimental points for all complexes (see Figures 3a and 6). Although the magnitude of the J_3 interaction is small, it cannot be neglected, as in many

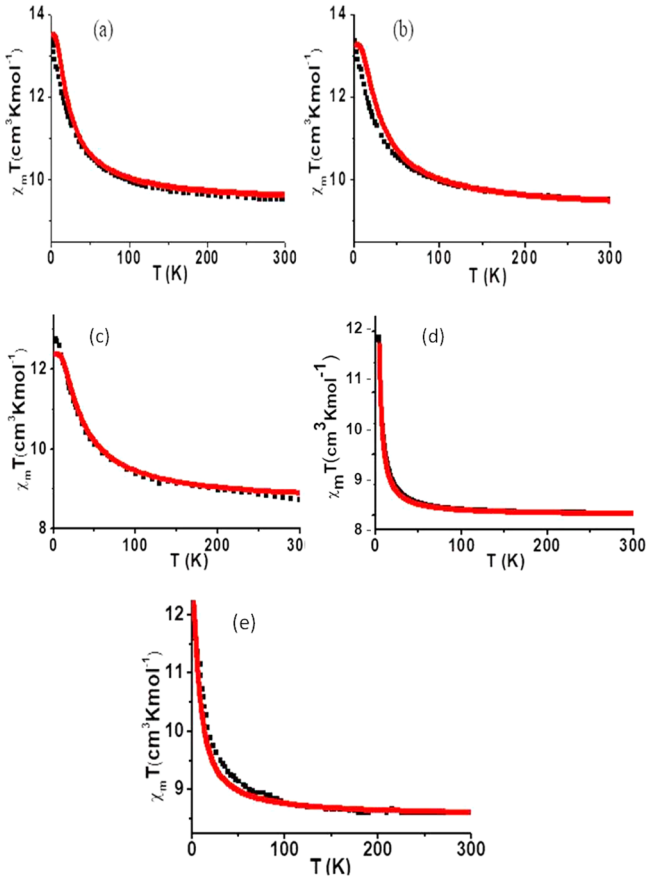

Figure 6. Experimental (black squares) and simulated (red squares) magnetic susceptibility curves for complexes (a) **1**, (b) **2**, (c) **3**, (d) **4**, and (e) **5**. Note here that the experimental data for complexes **1**–**5** have been reported earlier[12−15] and here they have been reproduced to show the match between the two sets.

DOI: 10.1021/acs.inorgchem.7b02775
Inorg. Chem. 2018, 57, 1846−1858

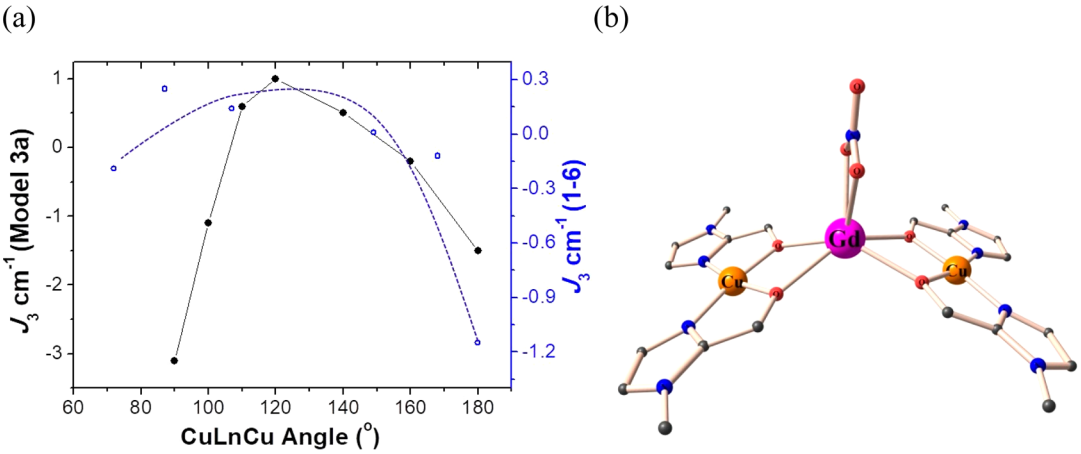

Figure 7. (a) Magnetostructural correlations for the next-nearest-neighbor (1,3) {Cu-Cu} interaction (J_3), developed on model **3a** with respect to the Cu−Gd−Cu angle. Solid black circles represent J_3 values calculated using the {Cu^{II}-Gd^{III}-Cu^{II}} model, while open blue circles represent DFT calculated values for complexes **1**−**6**. (b) Molecular structure for model **3a**. Color code: Gd, pink; Cu, golden yellow; O, brick red; N, blue; C, gray. H atoms are omitted for clarity.

cases the magnitudes of J_1 and J_2 are small. This is particularly important when the J_3 interaction is antiferromagnetic in nature and can bring the excited states closer to the ground state and hence enhances the MCE characteristics.

It should be noted here that when the experimental susceptibility data of complexes **1**−**6** are fitted, the $J_1 = J_2$ scenario is assumed; however, our calculations reveal a $J_1 \neq J_2$ scenario for complexes **1**−**4**. This is essentially due to the fact that the structural parameters associated with J_1 and J_2 interactions are different in complexes **1**−**4** (see Table 1). In particular, the {Cu-Gd} magnetic coupling is strongly correlated to the Cu−O−Gd bond angles and Cu−O−Gd−O dihedral angles. In complexes **1**−**6**, the Cu−O−Gd bond angles are found to be in the range of 96.4−110.0°. The Cu−O−Gd−O dihedral angles are found to be in the range of 0.7−21.0°. Magnetostructural correlations developed for the {Cu(OR)$_2$Gd} pair[8a,10e] utilizing both the bond angles and dihedral angles suggest that the J values should be in the range of +0.2 to +4.0 cm^{-1} for complexes **1**−**6**, and this is in accordance with both the experimental and computed values (see Figure S3 in the Supporting Information for the correlations).

In complexes **1** and **2**, the Cu$_1$−O−Gd angles and Cu$_1$−O−Gd−O dihedral angles are very close to each other (see Table 1); this leads to very similar J_1 values (3.22 and 3.40 cm^{-1} for complexes **1** and **2**, respectively). However, if we analyze J_2 interactions, substantial differences in the dihedral angles are visible (Cu$_2$−O−Gd−O dihedral angles are 21.0 and 12.4° for complexes **1** and **2**, respectively) and this leads to a substantial difference in the J_2 estimate (2.01 and 3.19 cm^{-1} for complexes **1** and **2**, respectively). This is also in accord with the magnetostructural correlation developed where a larger Cu−O−Gd−O dihedral angle leads to weaker ferromagnetic coupling (see Figure S3 in the Supporting Information). In complex **3**, Cu1−O−Gd and Cu2−O−Gd bond angles are very similar with a small variation in the dihedral angles (Cu$_1$−O−Gd−O and Cu$_2$−O−Gd−O dihedral angles are 1.9 and 3.4° for J_1 and J_2, respectively). With a smaller dihedral angle expected to yield stronger ferromagnetic coupling (3.86 and 3.78 cm^{-1} for J_1 and J_2, respectively), the minor variation observed in the J values can be rationalized. In comparison to complexes **1** and **2**, in complex **3** the Cu−O−Gd bond angles are larger (by ∼2−4°) and Cu−O−Gd−O dihedral angles are smaller (by ∼11−19°). Magnetostructural studies suggest a stronger ferromagnetic {Gd-Cu} interaction at smaller Cu−O−Gd−O dihedral angles and smaller Cu−O−Gd bond angles (in the range 97−115°; see Figure S3 in the Supporting Information). A larger change in Cu−O−Gd−O dihedral angles leads to relatively stronger ferromagnetic J_1 and J_2 values for complex **3** in comparison to complexes **1** and **2**.

For complex **4**, the Cu−O−Gd bond angles (106.8−109.7°) and Cu−O−Gd−O dihedral angles (5.7 and 11.3°) are found to be larger in comparison to those in complex **3**, resulting in smaller {Gd-Cu} ferromagnetic interactions (0.88 and 0.95 cm^{-1} for J_1 and J_2, respectively; see Figure S3 in the Supporting Information). The small difference in magnitude of J_1 and J_2 for complex **4** can be attributed to minor variation in the Cu−O−Gd−O dihedral angles. For complex **5**, the Cu−O−Gd bond angles (109−110°) are found to be very close to those in complex **4**, whereas Cu−O−Gd−O dihedral angles (0.7°) are found to be smaller in comparison, resulting in stronger {Gd-Cu} ferromagnetic interactions (1.06 cm^{-1}), as expected from the developed magnetostructural correlations. Complex **6** has the smallest Cu−O−Gd bond angles (96.4°) among all the six complexes, helping it to attain a large ferromagnetic {Gd-Cu} interaction, whereas the larger Cu−O−Gd−O dihedral angles (19.4°) cause reduction of the ferromagnetic {Gd-Cu} interaction and yield a moderate ferromagnetic {Gd-Cu} interaction (1.46 cm^{-1}).

In addition to the J_1 and J_2 interactions, the J_3 interaction should also be investigated carefully. The fit to the experimental susceptibility data performed earlier for complexes **1**−**3** reveal large next-nearest-neighbor interactions. The two Cu^{II} centers are not directly connected by the ligands in these complexes, and therefore the exchange is expected to be mediated via the Gd^{III} ion and hence is likely to be rather weak. The low-temperature region of the susceptibility data is found to be very sensitive to the sign and magnitude of the J_3 interactions, and our calculated values satisfactorily reproduce these data, offering confidence in the estimated sign/magnitude of the J_3 interactions.

Mechanism of Exchange Coupling. The mechanism of magnetic coupling for the {Cu-Gd} pair has been developed by some of us earlier.[8a,10e] Here we intend to extend the discussion

DOI: 10.1021/acs.inorgchem.7b02775
Inorg. Chem. 2018, 57, 1846−1858

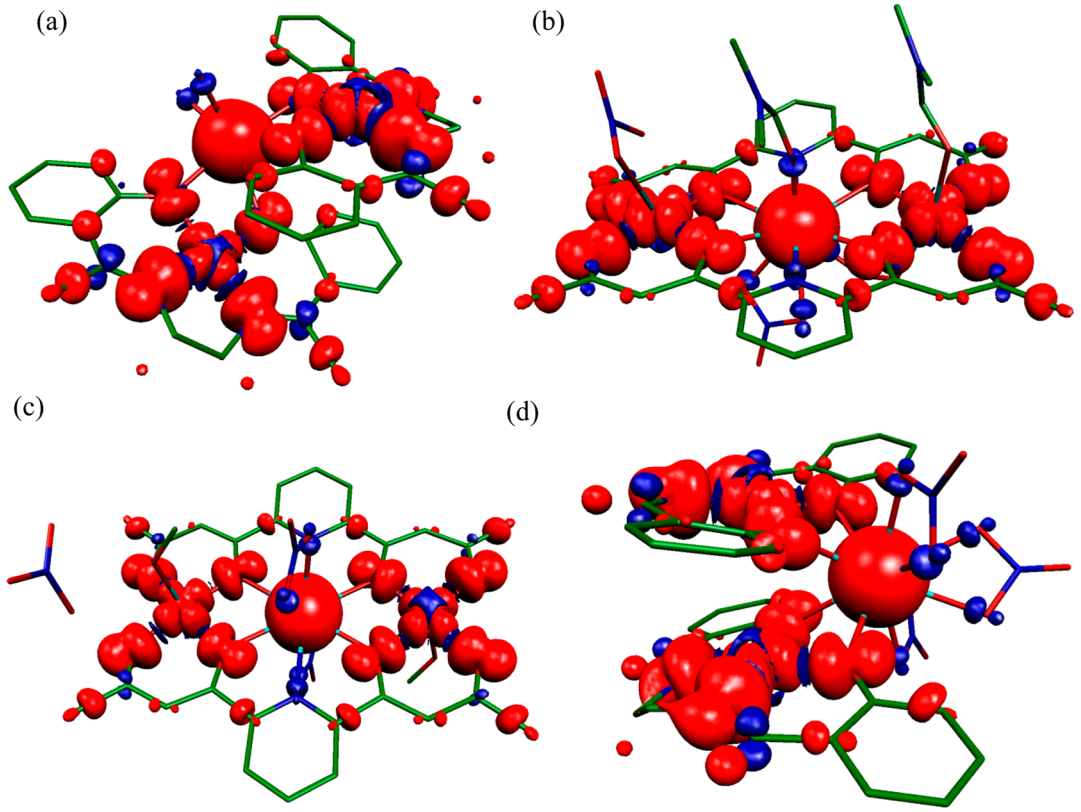

Figure 8. DFT computed spin density plots of (a) **2**, (b) **4**, (c) **5**, and (d) **6** for the $S = 9/2$ state. The isodensity surface represented corresponds to a value of 0.001 e/bohr^3. The red and blue regions indicate positive and negative densities.

to the {Cu-Gd-Cu} motif. The presence of two Cu^{II} ions on both sides of the Gd^{III} ion lead to a greater degree of overlap between the two sets (Cu^{II} $3d_{x^2-y^2}$ orbitals with the 5d, 6s, and 6p empty orbitals of the Gd^{III} ion). Since the charge transfer from the Cu^{II} to 5d, 6s, and 6p empty orbitals of Gd^{III} dominates the ferromagnetic part of the coupling, both the {Cu_A-Gd} and {Gd-Cu_B} interactions should have the same sign.

Calculations yield ferromagnetic J_3 interactions for complex **2**, while there is no significant interaction in complex **3** and complexes **1** and **4**−**6** have antiferromagnetic interactions. Quite interestingly, when the magnitude of J_3 is compared with the Cu−Gd−Cu angle, it is clear that both smaller and larger angles yield antiferromagnetic J_3 interactions (see Figure 7a).

To further understand the variation in J_3 interaction, we have performed overlap integral calculations for complexes **1** and **2**, between $d_{x^2-y^2}$ orbitals of both Cu^{II} ions. Here the J_3 interaction is antiferromagnetic for the former and ferromagnetic for the latter. Overlap integral calculations on complexes **1** and **2** suggest a significant $|d_{x^2-y^2}|La^{III}|d_{x^2-y^2}|$ overlap for complex **1** in comparison to complex **2** (0.010 and 0.005 for complexes **1** and **2**, respectively; see Figure S4 in the Supporting Information). Since this overlap integral is directly proportional to the antiferromagnetic part of the exchange, the larger overlap observed in complex **1** leads to antiferromagnetic coupling while a weaker overlap in complex **2** leads to ferromagnetic J_3. This analysis can be extended to other complexes as well. Among complexes **1**−**6**, complex **5** exhibits a very strong antiferromagnetic J_3 interaction (-1.15 cm^{-1}). This is essentially due to the fact that here the two Cu^{II} centers are connected by the ligand, leading to an additional superexchange pathway and a stronger antiferromagnetic exchange. This is clearly visible in the computed spin density plots, where the $d_{x^2-y^2}$ orbital tends to promote strong delocalization of spin density through the aromatic ligands (see Figure 8 and the discussion below). A closer look at the structure of complex **4** reveals a similar scenario, as the ligand employed in complex **4** is same as that of complex **5**; however here the J_3 interaction is weaker. The Cu−Gd−Cu angle in complex **5** is found to be 180°, while in **4** this is found to be 168°, leading to less overlap between the $d_{x^2-y^2}$ orbitals of both Cu^{II} ions and hence a smaller J_3 value.

To ascertain the relationship between J_3 and the Cu−Gd−Cu angles, we have performed magnetostructural studies on a model structure of complex **3** (**3a** generated from complex **3**; see Figure 7) by varying the Cu−Gd−Cu angle from 90 to 180° and keeping other structural parameters the same. The computed points are parabolic with both smaller and larger angles yielding stronger antiferromagnetic exchange (see Figure 7a). This correlation clearly reveals that the {Cu-Cu} interaction is strongly dependent on the Cu−Gd−Cu angle. To further understand the origin of the sign and magnitude of the J_3 interaction, we have performed overlap calculations on {Cu^{II}-Gd^{III}-Cu^{II}} models. Overlap integral calculations suggest strong $|d_{x^2-y^2}|Gd^{III}|d_{x^2-y^2}|$ overlap at both smaller and larger Cu−Gd−Cu angles, yielding strong antiferromagnetic interactions (see Figure S5 in the Supporting Information).

We have tabulated spin densities of all the important atoms for complexes **1**−**6** in Table S3 in the Supporting Information. Computed spin density plots for complexes **2** and **4**−**6** are shown in Figure 8, possessing weak ferromagnetic, moderate antiferromagnetic, strong antiferromagnetic, and weak antiferromagnetic J_3 values, respectively. In general, the spin density of the Cu^{II} ion is found to be delocalized to the coordinating

DOI: 10.1021/acs.inorgchem.7b02775
Inorg. Chem. 2018, 57, 1846−1858

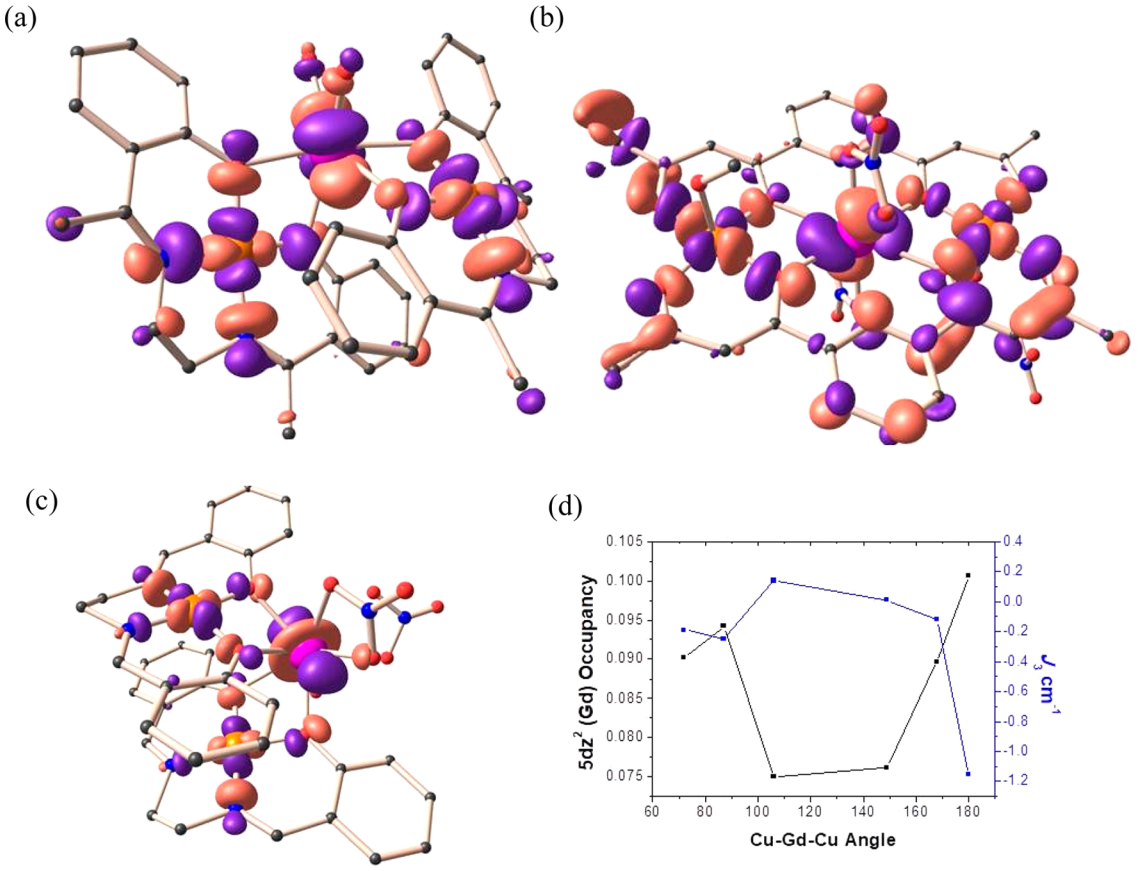

Figure 9. Molecular orbitals for complexes (a) **2**, (b) **5**, and (c) **6** showing $\{3d_{x^2-y^2}(Cu)\text{-}5d_{z^2}(Gd)\text{-}3d_{x^2-y^2}(Cu)\}$ orbital interaction. (d) NBO computed $5d_{z^2}(Gd)$ occupancy along with the J_3 interactions computed for complexes **1**–**6**.

atoms, while the Gd^{III} ion exhibits polarization, where it gains spin densities from the coordinating atoms. In all of these complexes, the Gd^{III} ion has a spin density value of ~7.02, whereas for the Cu^{II} ion this value is found to be in the range of 0.59–0.69.

To understand the sign and magnitude of the J_3 interactions, we have performed two sets of calculations. In the first set, calculations were performed using a Gd^{III} ion to extract J_3, and this value has been discussed above. Here the J_3 interaction is mediated via the Gd^{III} orbitals and we can expect that the valence orbitals of the Gd^{III} ion such as doubly occupied 5s and 5p orbitals, half-filled 4f orbitals, and the empty (5d, 6s, and 6p) orbitals are involved. To ascertain the role of 4f orbitals in magnetic coupling, we have replaced Gd^{III} by a La^{III} ion. Here we have used two types of basis sets for the La^{III} ion: the first basis set has 46 electrons in the core and 8 electrons in the valence shell, and in the second basis set, a large effective core potential containing all 54 electrons is employed. This is to ascertain particularly the role of filled 5s and 5p orbitals in the estimation of J values. Although minor variations are noted, these two sets of calculations yield very similar J_3 values (see Table 2) and this suggests that the occupied 5s and 5p core orbitals do not significantly influence the magnetic coupling. The difference in the computed values between the Gd^{III} set and La^{III} set reveals that the contributions arise due to the presence of $4f^7$ orbitals of the Gd^{III} ion. As the difference between these two sets is drastic, this suggests that $4f^7$ orbitals influence the J_3 interaction significantly. The net contributions to the exchange by the $4f^7$ orbitals are ferromagnetic in nature for complexes **1** and **4**–**6** while they are antiferromagnetic for complexes **2** and **3**. The overall sign of the J_3 interaction computed, however, is just opposite to the contributions arising from 4f orbitals, revealing that the empty 5d, 6s, and 6p orbitals play a dominant role in determining the sign of J_3 interactions. It is known that $4f^7$ orbitals via polarization contribute to the occupancy of the formally empty 5d orbitals, the absence of which (in La^{III} models) enhances overlap between the two $3d_{x^2-y^2}$ (Cu) orbitals, leading to stronger antiferromagnetic coupling for complexes **1** and **4**–**6**. The ferromagnetic couplings between two Cu^{II} centers in complexes **2** and **3** arise essentially due to orbital orthogonality. Here the presence of $4f^7$ orbitals tends to reduce the orthogonality between the two Cu^{II} orbitals by offering various {3d-4f} overlaps and hence contributing to the antiferromagnetic part of the exchange, leading to the reduction of net ferromagnetic coupling. This is supported by both the overlap calculations and also the NBO population analysis (see Table S4 and Figures S4 and S6 in the Supporting Information).

Among the 5d orbitals of Gd^{III}, the $5d_{z^2}$ orbital is particularly found to play a key role in controlling the magnitude of the {Cu-Cu} interaction. NBO analysis reveals an enhancement of occupancy of $5d_{z^2}$ orbitals for complexes possessing stronger antiferromagnetic coupling and vice versa. The Cu–Gd–Cu angle is found to control $\{3d_{x^2-y^2}(Cu)\text{-}5d_{z^2}(Gd)\text{-}3d_{x^2-y^2}(Cu)\}$ orbital interactions and thus control the magnitude and sign of the J_3 interaction (see Figure 9). In complex **2**, these orbitals are orthogonal to each other, leading to a ferromagnetic J_3 interaction (see Figure 9a). In complex **5**, we can see the maximum interaction between $\{3d_{x^2-y^2}(Cu)\text{-}5d_{z^2}(Gd)\text{-}3d_{x^2-y^2}(Cu)\}$ orbitals, leading to a very large antiferromagnetic

DOI: 10.1021/acs.inorgchem.7b02775
Inorg. Chem. 2018, 57, 1846–1858

Table 3. Calculated $-\Delta S_m$ Values Using DFT J Values Along with Their Maximum Attainable $-\Delta S_m$ Values in J kg^{-1} K^{-1}

complex	angle (Cu_1–Gd_3–Cu_2)	MW	$-\Delta S_{cal}$ @ 3 K, 7 T	$-\Delta S_m$(max)
1	87.2	1866.6	9.5	13.1
2	106.7	1941.2	9.1	12.6
3	148.9	1024.4	17.2	23.9
4	168.1	1217.1	15.9	20.1
5	180.0	1025.0	19.1	23.9
6	71.5	1003.0	17.9 (17.0[a])	24.4

[a]Experimental $-\Delta S_m$ value for complex **6** at 3.5 K and at a 7 T magnetic field.

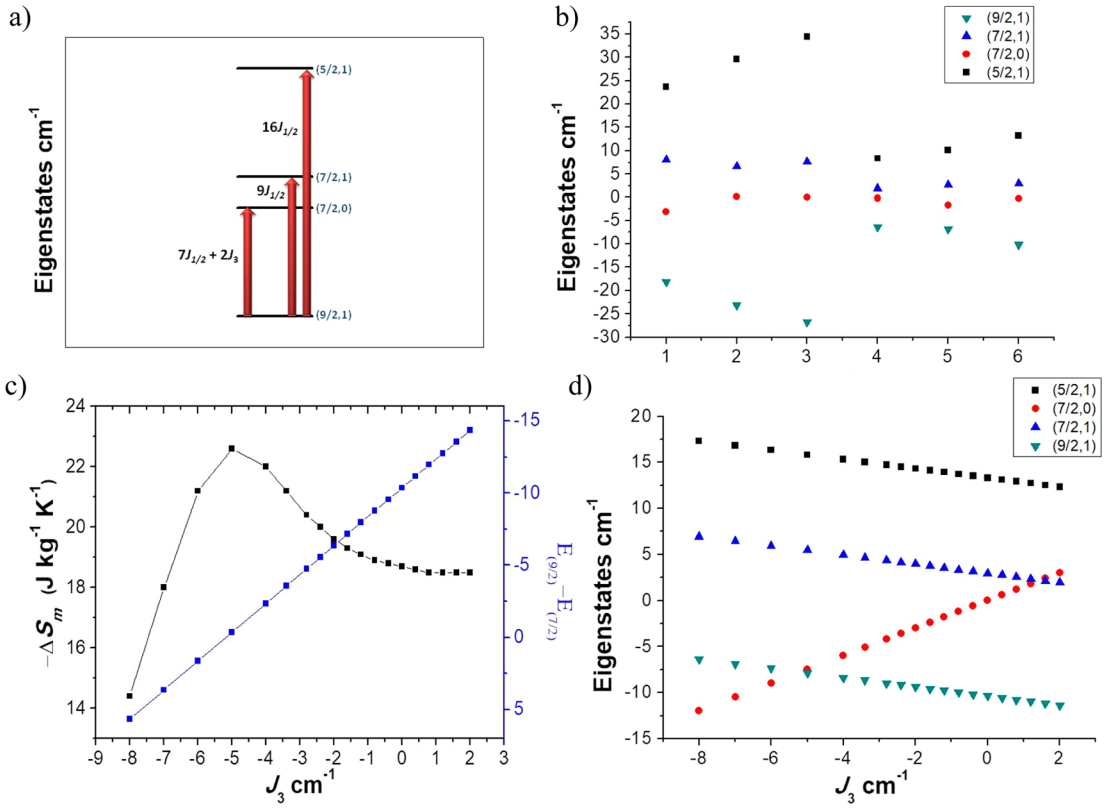

Figure 10. (a) Pictorial representation of eigenstates for **6**. (b) Eigenstate energy for complexes **1**–**6** at their respective calculated J values. (c) Variation of $-\Delta S_m$ values with respect to the J_3 values of **6**. (d) Eigenstate energy changes with respect to J_3 interactions.

J_3 interaction (see Figure 9b). However, in complex **6**, this overlap is found to be moderate, resulting in a weak antiferromagnetic coupling (see Figure 9c). The relationship between the magnitude of J_3 and the occupation value found for the $5d_{z^2}$ orbital is clearly reflected in the correlation developed (see Figure 9d).

As mentioned earlier, as we move through complexes **1**–**6**, the coordination numbers around the Cu^{II} and Gd^{III} ions vary. To check the influence of coordination number on the magnitude of the J_3 interaction, we have fictitiously modeled several structures from the X-ray structure of complex **4**, in which the coordination number around Cu^{II} ions was varied from 4 to 5 and that around the Gd^{III} ion was varied from 7 to 9. Calculations performed on these models are shown in Figure S7 in the Supporting Information, and only minor variations are noted in the J values, suggesting that the coordination number around the metal ion does not significantly influence the J values. This is also qualitatively rationalized on the basis of the fact that, for the Cu^{II} ion, ligands along the d_{z^2} direction do not play a significant role in the J values, as these orbitals are doubly occupied. As the $4f^7$ orbitals of Gd^{III} ion are deeply buried, their energies/overlaps are not significantly influenced by the ligand orbitals.

MCE of {Cu^{II}-Gd^{III}-Cu^{II}} Complexes. The ferromagnetic interaction prevailing between Cu^{II} and Gd^{III} ions in complexes **1**–**6** results in a large ground state and the isotropic nature of these ions directed us to probe the MCE characteristics. The entropy content for an uncoupled spin in the metal ions in a complex can be calculated using the following formulation $\sum_i R\ln(2s_i+1)$ and the corresponding values are shown in Table 3. The maximum attainable $-\Delta S_{max}$ values are found to be ~13–24 J kg^{-1} K^{-1} for these clusters, however experimentally $-\Delta S_m$ values have not been measured for complexes **1**–**5**. To understand how the computed exchange coupling influences the MCE values, we have computed $-\Delta S_m$ values for complexes **1**–**6** using DFT computed Js ($-\Delta S_{cal}$, see Table 3).

Experimentally complex **6** yields a $-\Delta S_m$ value of 17.0 J kg^{-1} K^{-1} at 3.5 K at a 7 T magnetic field and the $-\Delta S_{cal}$ value at the same temperature and magnetic field is estimated to be 17.5 J kg^{-1} K^{-1} (see Figure 4b). This striking match between the experimental and the calculated values offers confidence in the estimated $-\Delta S_{cal}$ values for complexes **1**–**5**. The {Cu-Gd}

DOI: 10.1021/acs.inorgchem.7b02775
Inorg. Chem. 2018, 57, 1846–1858

exchange interaction is estimated to be ferromagnetic in nature in all of the six complexes studied; however, the nature and strength of {Cu-Cu} interaction grossly varies. Assuming a $J_1 \approx J_2$ scenario, the energy gap between the ground (S = 9/2,1) (here 1 and 0 after the S values denoting the coupled spin states (triplet and singlet) of the two Cu^{II} centers in the Kambe vector coupling approach) and the first excited S = 7/2 (S = 7/2,0) states is given by $7J_1 + 2J_3$ (see Figure 10a); in order to have a large MCE, the S = 9/2 ground state and the first excited S = 7/2 state should be ideally degenerate. To achieve this, the J_3 interactions should be antiferromagnetic and 3.5 times larger than {Cu-Gd} coupling. For complexes **1**−**6**, the reported $-\Delta S_{cal}$ values are correlated to the $\Delta E(E_{S=9/2}-E_{S=7/2})$ gap, as shown in Figure 10b. This gap is found to have the order **5** < **4** < **6** < **1** < **2** < **3**, with complex **5** possessing the smallest gap and largest antiferromagnetic J_3 interaction. However, this order does not reflect the $-\Delta S_{cal}$ order observed among complexes **1**−**6** (**5** > **6** > **3** > **4** > **1** > **2**), and this is due to the following: (i) the molecular weights of the complexes are different, with a large molecular weight expected to yield smaller $-\Delta S_{cal}$ values, and (ii) the $J_1 \approx J_2$ scenario assumed is not strictly true for many complexes, resulting in another S = 7/2 state (S = 7/2,1) lying closer to the ground state and influencing the overall MCE computed.

The {Cu-Gd} coupling constants are difficult to control, as various structural parameters such as Cu−O−Gd angles and Cu−O−Gd−O dihedral angles influence this coupling constant. Here we intend to probe how the (1,3) {Cu-Cu} interactions are correlated to $-\Delta S_{cal}$ values. As the Cu−Gd−Cu angle is found to influence the J_3 interaction, we have developed a magnetostructural correlation for complex **6** where J_3 values are altered from −8.0 to +2.0 cm^{-1} (keeping the J_1 and J_2 values constant). Using this set of energy levels, both the $-\Delta S_{cal}$ and the $\Delta E(E_{S=9/2}-E_{S=7/2})$ values are estimated (see Figure 10c,d). As one moves from zero to larger antiferromagnetic interactions, $-\Delta S_{cal}$ values are found to increase until 5 cm^{-1} and then start to decrease (see Figure 10c). The maximum appears when the J_3 value is 3.5 times larger than the J_1/J_2 interactions, as at this point $\Delta E(E_{S=9/2}-E_{S=7/2})$ = 0. This trend can be explained by plotting the eigenstates with respect to J_3 interactions (see Figure 10d). As the J_3 exchange interaction becomes ferromagnetic, $-\Delta S_{cal}$ values tend to saturate, as at this point the J_3 interactions are not influencing MCE values. This clearly shows that the strong antiferromagnetic {Cu-Cu} exchange is a favorable aspect for $\{Cu^{II}$-Gd^{III}-$Cu^{II}\}$ complexes in enhanceingthe MCE values and this can be achieved by varying Cu−Gd−Cu angles. This angle can be easily controlled, as is evident from the literature examples, where this angle is found to vary from 71 to 180° in comparison to more resistive Cu−O−Gd/Cu−O−Gd−O angles.

CONCLUSIONS

To explore the importance of next-nearest-neighbor (1,3) {Cu-Cu} interactions, five trinuclear $\{Cu^{II}$-Gd^{III}-$Cu^{II}\}$ complexes have been chosen for DFT calculations. Additionally, a novel $\{Cu^{II}$-Gd^{III}-$Cu^{II}\}$ trinuclear complex has been synthesized and characterized. The conclusions derived from this work are summarized below.

(1) Computed {Cu-Gd} magnetic coupling constants for all the complexes are found to be ferromagnetic in nature and are in good agreement with experimentally reported values. The next-nearest-neighbor (1,3) {Cu-Cu} interaction, on the other hand, has been neglected or overestimated in the experimental fits. DFT studies suggest that the {Cu-Cu} interaction across the structures studied varies from small ferromagnetic to moderate antiferromagnetic coupling, and an excellent match between the susceptibility computed using DFT J values and experimental points add further support to the computed results.

(2) We have explored the mechanism of magnetic coupling for the $\{Cu^{II}$-Gd^{III}-$Cu^{II}\}$ motif. In particular, our calculations reveal that the net contribution to the (1,3) {Cu-Cu} exchange by the Gd^{III} $4f^7$ orbitals is ferromagnetic in nature for complexes **1** and **4**−**6** while it is antiferromagnetic for complexes **2** and **3**. The overall sign of (1,3) {Cu-Cu} exchange computed is opposite to the contributions arising from Gd^{III} $4f^7$ orbitals, suggesting how formally empty 5d, 6s, and 6p orbitals of Gd^{III} play a dominating role in determining the sign of this interaction.

(3) For complex **6**, the DFT computed J values offer an excellent fit to the experimental data, revealing a parameter-free approach to simulate the magnetic susceptibility even for such a small cluster. Magnetic, EPR, and computational studies on complex **6** suggest S = 9/2 to be the ground state. EPR simulations yield g = 1.99, D = 0.01 cm^{-1}, and E = 0.003 cm^{-1} parameters for the S = 9/2 ground state, whereas g = 2.5, D = 0.18 cm^{-1}, and E = 0.022 cm^{-1} parameters are found for the S = 7/2 first excited state. Experimentally, complex **6** yields an $-\Delta S_m$ value of 17.0 J kg^{-1} K^{-1} at 3.5 K employing a 7 T magnetic field and the $-\Delta S_{cal}$ value at the same temperature and magnetic field is estimated to be 17.5 J kg^{-1} K^{-1}. This reveals a striking match between experimental and calculated values and offers confidence in our computational methodology.

(4) The magnetostructural correlation developed by varying the Cu−Gd−Cu angle for J_3 exchange yields a parabolic behavior with both smaller and larger angles yielding antiferromagnetic coupling. When this interaction is antiferromagnetic and sufficiently large in comparison to the {Cu-Gd} coupling, this competes with the {Cu-Gd} interactions and lowers the energy gap between the S = 9/2 ground state and the S = 7/2 first excited state. To have a large MCE, degeneracy between S = 9/2 and S = 7/2 is desired, and this can be achieved when the (1,3) {Cu-Cu} interaction is antiferromagnetic and is 3.5 times larger than {Cu-Gd} coupling. Possession of a small ferromagnetic {Cu-Gd} coupling along with a smaller/larger Cu−Gd−Cu angle is likely to yield stronger antiferromagnetic (1,3) {Cu-Cu} interactions and hence can offer large MCE. Attempts to further improve the MCE within this class of molecules are underway in our laboratory.

ASSOCIATED CONTENT

Supporting Information

The Supporting Information is available free of charge on the ACS Publications website at DOI: 10.1021/acs.inorgchem.7b02775.

Crystallographic parameters, spin density and NBO plots, chemical formula structure, EPR spectra, magnetostructural correlation, and overlap integrals (PDF)

Accession Codes

CCDC 1565951 contains the supplementary crystallographic data for this paper. These data can be obtained free of charge via www.ccdc.cam.ac.uk/data_request/cif, or by emailing data_request@ccdc.cam.ac.uk, or by contacting The Cambridge

DOI: 10.1021/acs.inorgchem.7b02775
Inorg. Chem. 2018, 57, 1846−1858

Crystallographic Data Centre, 12 Union Road, Cambridge CB2 1EZ, UK; fax: +44 1223 336033.

AUTHOR INFORMATION

Corresponding Author

*G.R.: tel, (+91)-22-2576-7183. Email: rajaraman@chem.iitb.ac.in.

ORCID

Gopalan Rajaraman: 0000-0001-6133-3026

Notes

The authors declare no competing financial interest.

ACKNOWLEDGMENTS

G.R. thanks the SERB (EMR/2014/00024) and INSA for funding. M.K.S. thanks the UGC-India for a fellowship. T.R., R.K., and S.K.S. thank the CSIR-INDIA for fellowships.

REFERENCES

(1) Evangelisti, M.; Brechin, E. K. Recipes for enhanced molecular cooling. *Dalton Trans.* **2010**, *39*, 4672−4676.

(2) Giauque, W. F. A thermodynamic treatment of certain magnetic effects. A proposed method of producing temperatures considerably below 1° absolute. *J. Am. Chem. Soc.* **1927**, *49*, 1864.

(3) Sessoli, R. Chilling with Magnetic Molecules. *Angew. Chem., Int. Ed.* **2012**, *51*, 43.

(4) (a) Chen, Y. C.; Guo, F. S.; Liu, J. L.; Leng, J. D.; Vrábel, P.; Orendáč, M.; Prokleška, J.; Sechovský, V.; Tong, M. L. Switching of the Magnetocaloric Effect of Mn^{II}Glycolate by Water Molecules. *Chem. - Eur. J.* **2014**, *20*, 3029. (b) Lorusso, G.; Jenkins, M.; González-Monje, P.; Arauzo, A.; Sesé, J.; Ruiz-Molina, D.; Roubeau, O.; Evangelisti, M. Surface-Confined Molecular Coolers for Cryogenics. *Adv. Mater. (Weinheim, Ger.)* **2013**, *25*, 2984.

(5) (a) Zhang, Z. M.; Pan, L. Y.; Lin, W. Q.; Leng, J. D.; Guo, F. S.; Chen, Y. C.; Liu, J. L.; Tong, M. L. Wheel-shaped nanoscale 3d−4f $\{Co^{II}_{16}Ln^{III}_{24}\}$ clusters (Ln = Dy and Gd). *Chem. Commun.* **2013**, *49*, 8081. (b) Evangelisti, M.; Roubeau, O.; Palacios, E.; Camón, A.; Hooper, T. N.; Brechin, E. K.; Alonso, J. J. Cryogenic Magnetocaloric Effect in a Ferromagnetic Molecular Dimer. *Angew. Chem., Int. Ed.* **2011**, *50*, 6606−6609. (c) Guo, F. S.; Leng, J. D.; Liu, J. J.; Meng, Z. S.; Tong, M. L. Polynuclear and Polymeric Gadolinium Acetate Derivatives with Large Magnetocaloric Effect. *Inorg. Chem.* **2012**, *51*, 405. (d) Sharples, J. W.; Zheng, Y. Z.; Tuna, F.; McInnes, E. J. L.; Collison, D. Lanthanide discs chill well and relax slowly. *Chem. Commun.* **2011**, *47*, 7650. (e) Chang, L. X.; Xiong, G.; Wang, L.; Cheng, P.; Zhao, B. A 24-Gd nanocapsule with a large magnetocaloric effect. *Chem. Commun.* **2013**, *49*, 1055. (f) Hooper, T. N.; Schnack, J.; Piligkos, S.; Evangelisti, M.; Brechin, E. K. The importance of being exchanged: [Gd(III)4M(II)8(OH)8(L)8(O2CR)8]4+ clusters for magnetic refrigeration. *Angew. Chem., Int. Ed.* **2012**, *51*, 4633. (g) Jia, J. M.; Liu, S. J.; Cui, Y.; Han, S. D.; Hu, T. L.; Bu, X. H. 3D Gd^{III} Complex Containing Gd_{16} Macrocycles Exhibiting Large Magnetocaloric Effect. *Cryst. Growth Des.* **2013**, *13*, 4631.

(6) (a) Rajeshkumar, T.; Singh, S. K.; Rajaraman, G. A computational perspective on magnetic coupling, magneto-structural correlations, and magneto-caloric effect of a ferromagnetically coupled {GdIII−GdIII} Pair. *Polyhedron* **2013**, *52*, 1299−1305. (b) Canadillas-Delgado, L.; Fabelo, O.; Pasan, J.; Delgado, F. S.; Lloret, F.; Julve, M.; Ruiz-Perez, C. Intramolecular Ferro- and antiferromagnetic interactions in oxo-carboxylate bridged digadolinium(III) complexes. *Dalton Trans.* **2010**, *39*, 7286.

(7) (a) Costes, J.-P.; Dahan, F.; Dupuis, A.; Laurent, J.-P. Is Ferromagnetism an Intrinsic Property of the CuII/GdIII Couple? 1. Structures and Magnetic Properties of Two Novel Dinuclear Complexes with a μ-Phenolato−μ-Oximato (Cu, Gd) Core. *Inorg. Chem.* **2000**, *39*, 169−173. (b) Costes, J.-P.; Dahan, F.; Dupuis, A. Is Ferromagnetism an Intrinsic Property of the CuII/GdIII Couple? 2. Structures and Magnetic Properties of Novel Trinuclear Complexes with μ-Phenolato-μ-oximato (Cu−Ln−Cu) Cores (Ln = La, Ce, Gd). *Inorg. Chem.* **2000**, *39*, 5994−6000.

(8) (a) Rajaraman, G.; Totti, F.; Bencini, A.; Caneschi, A.; Sessoli, R.; Gatteschi, D. Density functional studies on the exchange interaction of a dinuclear Gd(iii)-Cu(ii) complex: Method assessment, magnetic coupling mechanism and magneto-structural correlations. *Dalton Trans.* **2009**, 3153−3161. (b) Cirera, J.; Ruiz, E. Exchange coupling in CuIIGdIII dinuclear complexes: A theoretical perspective. *C. R. Chim.* **2008**, *11*, 1227−1234.

(9) (a) Cremades, E.; Gómez-Coca, S.; Aravena, D.; Alvarez, S.; Ruiz, E. Theoretical Study of Exchange Coupling in 3d-Gd Complexes: Large Magnetocaloric Effect Systems. *J. Am. Chem. Soc.* **2012**, *134*, 10532−10542. (b) Langley, S. K.; Chilton, N. F.; Moubaraki, B.; Hooper, T.; Brechin, E. K.; Evangelisti, M.; Murray, K. S. Molecular coolers: The case for $[Cu^{II}_5Gd^{III}_4]$. *Chem. Sci.* **2011**, *2*, 1166. (c) Zheng, Y. Z.; Evangelisti, M.; Winpenny, R. E. P. Co−Gd phosphonate complexes as magnetic refrigerants. *Chem. Sci.* **2011**, *2*, 99. (d) Zheng, Y. Z.; Evangelisti, M.; Winpenny, R. E. P. *Angew. Chem., Int. Ed.* **2011**, *50*, 3692. (e) Karotsis, G.; Kennedy, S.; Teat, S. J.; Beavers, C. M.; Fowler, D. A.; Morales, J. J.; Evangelisti, M.; Dalgarno, S. J.; Brechin, E. K. Mn(4)(III)Ln(4)(III) Calix 4 arene Clusters as Enhanced Magnetic Coolers and Molecular Magnets. *J. Am. Chem. Soc.* **2010**, *132*, 12983−12990. (f) Peng, J. B.; Zhang, Q. C.; Kong, X. J.; Zheng, Y. Z.; Ren, Y. P.; Long, L. S.; Huang, R. B.; Zheng, L. S.; Zheng, Z. P. High-Nuclearity 3d−4f Clusters as Enhanced Magnetic Coolers and Molecular Magnets. *J. Am. Chem. Soc.* **2012**, *134*, 3314. (g) Guo, F. S.; Chen, Y. C.; Liu, J. L.; Leng, J. D.; Meng, Z. S.; Vrabel, P.; Orendac, M.; Tong, M. L. A large cryogenic magnetocaloric effect exhibited at low field by a 3D ferromagnetically coupled Mn(II)−Gd(III) framework material. *Chem. Commun.* **2012**, *48*, 12219. (h) Dermitzaki, D.; Lorusso, G.; Raptopoulou, C. P.; Psycharis, V.; Escuer, A.; Evangelisti, M.; Perlepes, S. P.; Stamatatos, T. C. Molecular Nanoscale Magnetic Refrigerants: A Ferrimagnetic $\{Cu^{II}_{15}Gd^{III}_7\}$ Cagelike Cluster from the Use of Pyridine-2,6-dimethanol. *Inorg. Chem.* **2013**, *52*, 10235. (i) Hooper, T. N.; Inglis, R.; Palacios, M. A.; Nichol, G. S.; Pitak, M. B.; Coles, S. J.; Lorusso, G.; Evangelisti, M.; Brechin, E. K. CO_2 as a reaction ingredient for the construction of metal cages: a carbonate-panelled $[Gd_6Cu_3]$ tridiminished icosahedron. *Chem. Commun.* **2014**, *50*, 3498. (j) Peng, J. N.; Zhang, Q. Q.; Kong, X. L.; Long, L. S.; Huang, R. B.; Zheng, L. S.; Zheng, Z. A 48-metal cluster exhibiting a large magnetocaloric effect. *Angew. Chem., Int. Ed.* **2011**, *50*, 10649. (k) Zheng, Y. Z.; Moreno Pineda, E.; Helliwell, M.; Winpenny, R. E. P. Mn^{II}−Gd^{III} Phosphonate Cages with a Large Magnetocaloric Effect. *Chem. - Eur. J.* **2012**, *18*, 4161. (l) Pineda, E. M.; Tuna, F.; Pritchard, R. G.; Regan, A. C.; Winpenny, R. E. P.; McInnes, E. J. L. Molecular amino-phosphonate cobalt−lanthanide clusters. *Chem. Commun.* **2013**, *49*, 3522. (m) Birk, T.; Pedersen, K. S.; Thuesen, C. A.; Weyhermüller, T.; Schau-Magnussen, M.; Poligkos, S.; Weihe, H.; Mossin, S.; Evangelisti, M.; Bendix, J. Fluoride Bridges as Structure-Directing Motifs in 3d-4f Cluster Chemistry. *Inorg. Chem.* **2012**, *51*, 5435. (n) Zheng, Y. Z.; Evangelisti, M.; Tuna, F.; Winpenny, R. E. P. Co−Ln Mixed-Metal Phosphonate Grids and Cages as Molecular Magnetic Refrigerants. *J. Am. Chem. Soc.* **2012**, *134*, 1057.

(10) (a) Liu, J. L.; Chen, Y. C.; Li, Q. W.; Gómez-Coca, S.; Aravena, D.; Ruiz, E.; Lin, W. Q.; Leng, J. D.; Tong, M. L. Two 3d-4f nanomagnets formed via a two-step in situ reaction of picolinaldehyde. *Chem. Commun.* **2013**, *49*, 6549−6551. (b) Liu, J. L.; Lin, W. Q.; Chen, Y. C.; Gõmez-Coca, S.; Aravena, D.; Ruiz, E.; Leng, J. D.; Tong, M. L. CuII - GdIII cryogenic magnetic refrigerants and Cu_8Dy_9 single-molecule magnet generated by in situ reactions of picolinaldehyde and acetylpyridine: Experimental and theoretical study. *Chem. - Eur. J.* **2013**, *19*, 17567−17577. (c) Leng, J. D.; Liu, J. L.; Tong, M. L. Unique nanoscale $\{Cu^{II}_{36}Ln^{III}_{24}\}$ (Ln = Dy and Gd) metallo-rings. *Chem. Commun.* **2012**, *48*, 5286. (d) Dinca, A. S.; Ghirri, A.; Madalan, A. M.; Affronte, M.; Andruh, M. Dodecanuclear $[Cu^{II}_6Gd^{III}_6]$ Nanoclusters as Magnetic Refrigerants. *Inorg. Chem.* **2012**, *51*, 3935. (e) Rajeshkumar, T.; Annadata, H. V.; Evangelisti, M.; Langley, S. K.; Chilton, N. F.;

DOI: 10.1021/acs.inorgchem.7b02775
Inorg. Chem. 2018, 57, 1846−1858

Murray, K. S.; Rajaraman, G. Theoretical Studies on Polynuclear {CuII5GdIIIn} Clusters (n = 4, 2): Towards Understanding Their Large Magnetocaloric Effect. *Inorg. Chem.* **2015**, *54*, 1661−1670.
(11) (a) Milios, C. J.; Manoli, M.; Rajaraman, G.; Mishra, A.; Budd, L. E.; White, F.; Parsons, S.; Wernsdorfer, W.; Christou, G.; Brechin, E. K. A Family of [Mn_6] Complexes Featuring Tripodal Ligands. *Inorg. Chem.* **2006**, *45*, 6782. (b) Rajaraman, G.; Cano, J.; Brechin, E. K.; McInnes, E. J. L. Density functional calculations of a tetradecametallic iron(iii) cluster with a very large spin ground state. *Chem. Commun.* **2004**, 1476−1477. (c) Rajeshkumar, T.; Rajaraman, G. Is a radical bridge a route to strong exchange interactions in lanthanide complexes? A computational examination. *Chem. Commun.* **2012**, *48*, 7856−7858. (d) Singh, S. K.; Pedersen, K. S.; Sigrist, M.; Thuesen, C. A.; Schau-Magnussen, M.; Mutka, H.; Piligkos, S.; Weihe, H.; Rajaraman, G.; Bendix, J. Angular dependence of the exchange interaction in fluoride-bridged Gd III-CrIII complexes. *Chem. Commun.* **2013**, *49*, 5583−5585. (e) Singh, S. K.; Rajaraman, G. Decisive interactions that determine ferro/antiferromagnetic coupling in {3d-4f} pairs: A case study on dinuclear {V(iv)-Gd(iii)} complexes. *Dalton Trans.* **2013**, *42*, 3623−3630. (f) Singh, S. K.; Tibrewal, N. K.; Rajaraman, G. Density functional studies on dinuclear {NiIIGdIII} and trinuclear {NiIIGdIIINiII} complexes: Magnetic exchange and magneto-structural maps. *Dalton Trans.* **2011**, *40*, 10897−10906. (g) Baker, M. L.; Timco, G. A.; Piligkos, S.; Mathieson, J. S.; Mutka, H.; Tuna, F.; Kozłowski, P.; Antkowiak, M.; Guidi, T.; Gupta, T.; Rath, H.; Woolfson, R. J.; Kamieniarz, G.; Pritchard, R. G.; Weihe, H.; Cronin, L.; Rajaraman, G.; Collison, D.; McInnes, E. J. L.; Winpenny, R. E. P. A classification of spin frustration in molecular magnets from a physical study of large odd-numbered-metal, odd electron rings. *Proc. Natl. Acad. Sci. U. S. A.* **2012**, *109*, 19113−19118.
(12) Bencini, A.; Benelli, C.; Caneschi, A.; Carlin, R. L.; Dei, A.; Gatteschi, D. Crystal and molecular structure of and magnetic coupling in two complexes containing gadolinium(III) and copper(II) ions. *J. Am. Chem. Soc.* **1985**, *107*, 8128.
(13) He, F.; Tong, M. L.; Chen, X. M. Synthesis, Structures, and Magnetic Properties of Heteronuclear Cu(II)−Ln(III) (Ln = La, Gd, or Tb) Complexes. *Inorg. Chem.* **2005**, *44*, 8285.
(14) Shiga, T.; Ohba, M.; Okawa, H. A Series of Trinuclear $Cu^{II}Ln^{III}Cu^{II}$ Complexes Derived from 2,6-Di(acetoacetyl)pyridine: Synthesis, Structure, and Magnetism. *Inorg. Chem.* **2004**, *43*, 4435.
(15) Shimada, T.; Okazawa, A.; Kojima, N.; Yoshii, S.; Nojiri, H.; Ishida, T. Ferromagnetic Exchange Couplings Showing a Chemical Trend in Cu−Ln−Cu Complexes (Ln = Gd, Tb, Dy, Ho, Er). *Inorg. Chem.* **2011**, *50*, 10555−10557.
(16) Noodleman, L. Valence Bond Description of Antiferromagnetic Coupling in Transition Metal Dimers. *J. Chem. Phys.* **1981**, *74*, 5737.
(17) Becke, A. D. Density-Functional Thermochemistry. III. The Role of Exact Exchange. *J. Chem. Phys.* **1993**, *98*, 5648.
(18) Schäfer, A.; Huber, C.; Ahlrichs, R. Fully optimized contracted Gaussian basis sets of triple zeta valence quality for atoms Li to Kr. *J. Chem. Phys.* **1994**, *100*, 5829.
(19) Cundari, T. R.; Stevens, W. J. Effective core potential methods for the lanthanides. *J. Chem. Phys.* **1993**, *98*, 5555−5565.
(20) Frisch, M. J.; Trucks, G. W.; Schlegel, H. B.; Scuseria, G. E.; Robb, M. A.; Cheeseman, J. R.; Scalmani, G.; Barone, V.; Mennucci, B.; Petersson, G. A.; Nakatsuji, H.; Caricato, M.; Li, X.; Hratchian, H. P.; Izmaylov, A. F.; Bloino, J.; Zheng, G.; Sonnenberg, J. L.; Hada, M.; Ehara, M.; Toyota, K.; Fukuda, R.; Hasegawa, J.; Ishida, M.; Nakajima, T.; Honda, Y.; Kitao, O.; Nakai, H.; Vreven, T.; Montgomery, J. A.; Peralta, J. E.; Ogliaro, F.; Bearpark, M.; Heyd, J. J.; Brothers, E.; Kudin, K. N.; Staroverov, V. N.; Kobayashi, R.; Normand, J.; Raghavachari, K.; Rendell, A.; Burant, J. C.; Iyengar, S. S.; Tomasi, J.; Cossi, M.; Rega, N.; Millam, J. M.; Klene, M.; Knox, J. E.; Cross, J. B.; Bakken, V.; Adamo, C.; Jaramillo, J.; Gomperts, R.; Stratmann, R. E.; Yazyev, O.; Austin, A.; Cammi, J. R.; Pomelli, C.; Ochterski, J. W.; Martin, R. L.; Morokuma, K.; Zakrzewski, V. G.; Voth, G. A.; Salvador, P.; Dannenberg, J. J.; Dapprich, S.; Daniels, A. D.; Farkas, Ö.; Foresman, J. B.; Ortiz, J. V.; Cioslowski, J.; Fox, D. J. *Gaussian 09*; Gaussian, Inc., Wallingford, CT, 2009.
(21) Borras-Almenar, J. J.; Clemente-Juan, J. M.; Coronado, E.; Tsukerblat, B. S. MAGPACK[1] A package to calculate the energy levels, bulk magnetic properties, and inelastic neutron scattering spectra of high nuclearity spin clusters. *J. Comput. Chem.* **2001**, *22*, 985.
(22) Chilton, N. F.; Anderson, R. P.; Turner, L. D.; Soncini, A.; Murray, K. S. PHI: A powerful new program for the analysis of anisotropic monomeric and exchange-coupled polynuclear *d*- and *f*-block complexes. *J. Comput. Chem.* **2013**, *34*, 1164.
(23) Kahn, M. L.; Rajendiran, T. M.; Jeannin, Y.; Mathonière, C.; Kahn, O. LnIIICuII Schiff base compounds (Ln = Ce, Gd, Tb, Dy, Ho, Er): structural and magnetic properties. *C. R. Acad. Sci., Ser. IIc: Chim.* **2000**, *3*, 131−137.
(24) Stoll, S.; Schweiger, A. EasySpin, a comprehensive software package for spectral simulation and analysis in EPR. *J. Magn. Reson.* **2006**, *178*, 42−55.
(25) Gruber, S. J.; Harris, C. M.; Sinn, E. Metal complexes as ligands—IV [1,2,3]: Bi- and Tri- nuclear complexes derived from metal complexes of tetradentate salicylaldimines. *J. Inorg. Nucl. Chem.* **1968**, *30*, 1805.
(26) Kambe, K. On the paramagnetic susceptibilities of some polynuclear complex salts. *J. Phys. Soc. Jpn.* **1950**, *5*, 48−51.

DOI: 10.1021/acs.inorgchem.7b02775
Inorg. Chem. 2018, 57, 1846−1858